Published in final edited form as:

Immunity. 2015 September 15; 43(3): 579–590. doi:10.1016/j.immuni.2015.08.006.

Regulatory T cells in tumor-associated tertiary lymphoid structures suppress anti-tumor T cell responses

Nikhil S. Joshi[1], **Elliot H. Akama-Garren**[1], **Yisi Lu**[1], **Da-Yae Lee**[1], **Gregory P. Chang**[1], **Amy Li**[1], **Michel DuPage**[1], **Tuomas Tammela**[1], **Natanya R. Kerper**[1], **Anna F. Farago**[1], **Rebecca Robbins**[1], **Denise M. Crowley**[1], **Roderick T. Bronson**[3], and **Tyler Jacks**[1,2,§]

[1]Koch Institute for Integrative Cancer Research and Department of Biology, Massachusetts Institute of Technology, Cambridge, MA 02142

[2]Howard Hughes Medical Institute, Massachusetts Institute of Technology, Cambridge, MA 02142

[3]Department of Pathology, Tufts University School of Medicine and Veterinary Medicine, North Grafton, Massachusetts 01536, USA

[4]Cancer Center and Department of Pathology, Massachusetts General Hospital, Boston, MA 02114

SUMMARY

Infiltration of regulatory T (Treg) cells into many tumor types correlates with poor patient prognoses. However, mechanisms of intratumoral Treg cell function remain to be elucidated. We investigated Treg cell function in a genetically-engineered mouse lung adenocarcinoma model and found Treg cells suppress anti-tumor responses in tumor-associated tertiary lymphoid structures (TA-TLS). TA-TLS have been described in human lung cancers, but their function remains to be determined. TLS in this model were spatially associated with >90% of tumors and facilitated interactions between T cells and tumor-antigen presenting dendritic cells (DCs). Costimulatory ligand expression by DCs and T cell proliferation rates increased in TA-TLS upon Treg cell depletion, leading to tumor destruction. Thus, we propose Treg cells in TA-TLS can inhibit endogenous immune responses against tumors, and targeting these cells may provide therapeutic benefit for cancer patients.

INTRODUCTION

Non-small cell lung cancer (NSCLC), including lung adenocarcinoma, accounts for ~25% of all cancer deaths (Jemal et al., 2010), and, despite improvements in therapy, NSCLC mortality remains around 80% (http://seer.cancer.gov/statfacts/html/lungb.html). Immunotherapy uses the immune system to attack cancer and has demonstrated durable tumor regression in “immunogenic” tumor types like melanoma (Pardoll, 2012). Yet, until

§**CONTACT** Author for correspondence: tjacks@mit.edu.

Author Contribution

N.S.J. and T.J. designed the study, and N.S.J. wrote the manuscript. N.S.J., E.H.A-G., Y.L., D-Y.L., G.P.C., A.L., R.R., D.M.C., and A.F.F. generated primary data. M.D. initiated the project. T.T. and N.R.K. established the CLARITY method in the laboratory. R.T.B. graded tumors. T.J. supervised data analysis and experiments.

recently, NSCLC was considered “non-immunogenic” because tumors responded poorly to immunotherapeutics (Raez et al., 2005). Furthermore, it was thought that lung tumors might not elicit strong endogenous T cell responses compared to melanoma, even though these tumor types had similar numbers of mutations and predicted neoantigens (Rajasagi et al., 2014; Vogelstein et al., 2013). The recent success of immune checkpoint inhibitors in NSCLC patients demonstrates that anti-tumor T cell responses do exist in a significant fraction of lung cancer patients, but they are functionally inhibited by poorly understood immunosuppressive mechanisms (Pardoll, 2012). Overcoming these mechanisms will be essential for generating more effective immunotherapies for this disease.

Regulatory T cell (Treg) deficiency, through mutation or deletion of the X-linked Forkhead box P3 (*Foxp3*) gene, leads to a fatal lymphoproliferative disease (Josefowicz et al., 2012). However, Treg cells may also facilitate tumor progression by suppressing adaptive immunity against tumors. Treg cell depletion in transplantable, carcinogen-induced, and autochthonous tumor models demonstrates increased anti-tumor immune responses, even against previously established tumors, which results in reductions in tumor size (Sakaguchi, 2004; Bos et al., 2013; Teng et al., 2010). Yet, many questions remain about how and where Treg cells function in the context of developing tumors.

Treg cells suppress self-reactive T cells in secondary lymphoid organs (SLOs; *e.g.* lymph nodes (LNs) and spleen). Similarly, Treg cells can suppress anti-tumor responses in tumor-draining LNs (Boissonnas et al., 2010; Campbell and Koch, 2011). However, Treg cells inside tumor tissues might also be important in natural tumor progression. Treg cells are often enriched in tumor tissue, and a high ratio of intratumoral Treg cells to effector T cells generally predicts poor patient outcomes (Fridman et al., 2012). Furthermore, the ability of anti-CTLA-4 antibodies to deplete intratumoral, but not LN, Treg cells is critical for their efficacy in animal cancer models (Marabelle et al., 2013; Selby et al., 2013; Simpson et al., 2013). However, while previous data suggest that intratumoral Treg cells promote tumor development, the mechanisms by which they do so remain to be fully determined.

In patients, across cancer types, lymphocytes can be found in LN-like, large, complex tumor-associated tertiary lymphoid structures (TA-TLS; Fridman et al., 2012; Goc et al., 2013). Amongst patients with early-stage NSCLC, ~70% have TA-TLS, which contain immune cells with an activated phenotype, similar to TLS observed after viral infection (Neyt et al., 2012; de Chaisemartin et al., 2011; Dieu-Nosjean et al., 2008). TA-TLS presence also correlates with increased overall survival. Thus, it is thought that TA-TLS promote anti-tumor responses. However, TA-TLS have not been described in animal models and their proposed functions have not been experimentally tested. It is also uncertain whether immunosuppressive pathways are active in TA-TLS.

Genetically-engineered mouse models (GEMMs) of cancer have greatly informed understanding of tumor biology and therapy (Hayes et al., 2014; Kwon and Berns, 2013). Tumors in GEMMs develop from untransformed cells in their native microenvironment, and, importantly, in the presence of a fully functional immune system. However, tumors in GEMMs are often poorly immunogenic and, consequentially, the use of GEMMs for tumor immunology studies has lagged (DuPage and Jacks, 2013). We previously programmed

autochthonous sarcomas and lung adenocarcinomas in “KP” mice (*Kras*$^{Lox\text{-}STOP\text{-}Lox\ (LSL)\text{-}G12D}$ *Trp53*$^{flox/flox}$) to express “LucOS”, firefly luciferase fused to a portion of ovalbumin (ova, encoding the potent T cell OT-I and OT-II antigens), and the antigenic 2C peptide (Dupage et al., 2011; DuPage et al., 2012). In both tumor types, tumor-specific T cells had a significant impact on tumor development, but disease outcomes differed. T cells prevented the development of LucOS-expressing sarcomas, and, consequentially, only “edited” (LucOS-negative) sarcomas developed (DuPage et al., 2012). In contrast, while T cells restrained the growth LucOS-expressing lung tumors early in disease course, they could not prevent it (Dupage et al., 2011). Moreover, this initial impact on tumor growth was followed by immune suppression, despite the confirmed expression of LucOS by tumors. Therefore, while sarcomas escaped immune control via editing, lung tumors escaped because the anti-tumor response itself was suppressed. The mediators of immunosuppression in the lung adenocarcinoma model are unknown. Because Treg cells are prominent in early LucOS-expressing tumors (Dupage et al., 2011), we reasoned that they might be important in immune suppression in later-stage tumors. Here we investigated the functions of intratumoral Treg cells in advanced lung adenocarcinomas.

RESULTS

Treg cells accumulate in tumor-bearing lungs and have an activated phenotype

To identify and deplete Treg cells in autochthonous lung tumors, we bred KP mice to *Foxp3*$^{IRES\text{-}DTR\text{-}GFP}$ mice (Kim et al., 2007), in which all CD4$^+$ FoxP3$^+$ Treg cells express diphtheria toxin receptor (DTR)-GFP fusion protein. Lung tumors in “KP-F” mice (*F: FoxP3*$^{DTR\text{-}GFP/DTR\text{-}GFP}$ or *KP-FoxP3*$^{DTR\text{-}GFP/y}$) were initiated by intratracheal (IT) administration of non-replicating lentiviruses co-expressing LucOS and Cre-recombinase (LucOS/Cre LV; Dupage et al., 2011). In lung epithelial cells, Cre activates oncogenic *Kras*^{G12D} and deletes *Trp53*, resulting in the development of autochthonous lung adenocarcinomas over a period of months (**Figure S1A**; Dupage et al., 2011). After 20-24 wks, KP-F mice had a mixture of low- and high-grade lung adenocarcinomas with few infiltrating lymphocytes (**Figure S1B**).

To identify circulating and lung-tissue Treg cells in flow cytometric analysis, we labeled the circulating cells with anti-CD45 (CD45$^{PE\text{-}CF594}$) antibodies injected prior to sacrifice (**Figure S1C**). In control 20-wk LucOS-infected P-F (*Kras*$^{+/+}$) mice, most “lung” CD4$^+$ T cells or Treg cells were in the circulation (CD45$^{PE\text{-}CF594+}$), but in tumor-bearing animals, a large fraction of the CD4$^+$ T cells and Treg cells were in the lung tissue (CD45$^{PE\text{-}CF594-}$; **Figure 1A**). This corresponded with a >20-fold increase in lung-tissue Treg cell number, while circulating Treg cell numbers remained unchanged (**Figure 1B**). Similar results were seen with excised tumors (data not shown).

Immunophenotyping demonstrated that ~60-80% of the lung-tissue Treg cells in tumor-bearing mice expressed CD103 (Integrin αE; **Figure 1C**), a marker of Treg cells found in sites of inflammation (Feuerer et al., 2010; Sather et al., 2007; Suffia et al., 2005). Furthermore, ~50% of the CD103$^+$ Treg cells also expressed the killer cell lectin-like receptor G1 (KLRG1), which is typically associated with terminally differentiated immune cells (Beyersdorf et al., 2007; Cheng et al., 2012; Joshi et al., 2007; Robbins et al., 2005). In

contrast, the presence of tumors did not affect CD103 and KLRG1 expression by Treg cells in the lung circulation, tumor-draining mediastinal LN (mLN), and control inguinal LN (iLN ;**Figure 1C**). $CD103^+$ $KLRG1^+$ double positive (DP) Treg cells expressed high amounts of several additional molecules previously associated with activated Treg cells, including two markers of T cell activation, CD44 and CD69, and the ectonucleotidase CD39 (**Figure 1D**). DP Treg cells also expressed high amounts of the IL-2 high-affinity receptor, IL-2Rα (CD25) as well as the immunoinhibitory receptor PD-1 (**Figure 1D**). The expression of these markers by DP Treg cells was higher than $CD103^+$ $KLRG1^-$ single positive (SP) or $CD103^-$ $KLRG1^-$ double negative (DN) Treg cells in the lung tissue (**Figure 1D**). Treg cells in lung tissue also expressed higher amounts of CTLA-4 than Treg cells in the mLN (**Figure 1E**). Together these data suggest that tumor-infiltrating Treg cells exhibit an activated phenotype, similar to Treg cells found at sites of inflammation. As few Treg cells with this phenotype were observed in the draining LN, it is likely that Treg cells acquired their activated phenotype within the tumor-bearing lung.

Treg cells actively suppress anti-tumor responses targeting established lung adenocarcinomas

We next assessed the effect of Treg cell depletion on tumors in KP-F mice. Two intraperitoneal (IP) injections of DT (50ug/g) into tumor-bearing (~18-20 wks post infection, pi) or non-tumor-bearing KP-F mice efficiently eliminated Treg cells in the lungs and lymphoid tissues (**Figure 2A** and **S2A-B**). However, *FoxP3*^{DTR} mice, but not *FoxP3*^{WT} mice, became moribund within ~2-3 weeks of depletion, requiring sacrifice (**Figure S2C**). Additionally, in tumor-bearing KP-*Foxp3*$^{DTR\text{-}GFP/+}$ (KP-F/+) mice, in which only 50% of all Treg cells express DTR-GFP due to X-inactivation (**Figure S2D**), DT treatment did not cause morbidity (data not shown). Therefore, the observed morbidity was caused by an autoimmune response triggered by transient Treg cell depletion and was not a side effect of DT treatment. Consistent with this, 12 days post depletion most T cells in KP-F mice, but not KP-F/+ mice, were activated ($CD44^{hi}$) and mice had dramatic lymphadenopathy and splenomegaly, with lymphocytic infiltration in several tissues throughout the body (**Figure S2E-H**; Kim et al., 2007). Of note, regardless of tumor status, we observed lymphocytic infiltration near the major airways in the lungs of Treg cell-depleted mice, accompanied by goblet cell metaplasia, similar to what is seen in FoxP3-deficient mice (**Figure S2I-J**; Lin et al., 2005). However, in non-tumor bearing animals, the alveolar spaces in the lungs (where tumors normally develop) were free from infiltration.

To track tumor cell fate after Treg cell depletion, KP-F mice were bred to *Rosa26*$^{LSL\text{-}tdTomato(tdT)}$ mice to generate “KPT-F” mice, in which Cre induces tdT expression in tumor cells (**Figure S1A**; Madisen et al., 2010). Immunofluorescence (IF) staining of tumors from untreated ~20wk KPT-F mice demonstrated they were composed of abundant, healthy-appearing tdT^+ tumor cells that were arranged primarily in papillary structures with EpCAM staining junctions between adjacent tumor cells (**Figure 2B**). In contrast, day-12 Treg cell-depleted tumors had a range of cellular infiltration and disruption of regular tissue architecture (**Figure 2B**). Quantification of 85 control and 108 Treg cell-depleted tumors showed >80% of the Treg cell-depleted tumors had moderate or severe disruption (**Figure 2C**). To visualize tumor destruction more comprehensively, we

performed CLARITY (Chung et al., 2013) on lungs from control and Treg cell-depleted KPT-F mice. This allowed whole tumor 3-dimensional (3-D) confocal imaging of 15 control and 10 Treg cell-depleted tumors. Tumors from the Treg cell-depleted mice showed extensive cellular infiltration (**Figure 2D** and **Movie S1**), and contained cavities filled with densely packed (non-tumor) cells. Furthermore, tumor cells in the Treg cell-depleted mice were thin and elongated and no longer formed connections with adjacent tumor cells (**Figure 2B** and **2D**). These data demonstrate that the cellular density and morphology of tumors were severely disrupted by Treg cell depletion.

Immunohistochemical (IHC) analysis showed that most of the infiltrating cells in Treg cell-depleted tumors were $CD45^+$ immune cells (**Figure 2E**). Infiltration was highly focused in the areas near tumors, as distal areas were free of immune infiltrates (**Figure S3A**). Immune infiltration was not observed in tumors from Treg cell-depleted KPT-F/+ mice, indicating that depletion of more than half of the Treg cell population was required for anti-tumor effects (**Figure S3B**). FACS analysis revealed the number of $CD4^+$ and $CD8^+$ T cells in the lung increased after Treg cell depletion (**Figure 2F**). In contrast, B cell number was not increased. IF analyses showed that in undepleted mice, $CD3^+$ T cells in tumors were primarily located within or near blood vessels, and $CD11c^+$ macrophages were located within airway-like pockets surrounded by tumor cells (**Figure S4AB**). In contrast, in the absence of Treg cells, $CD4^+$ and $CD8^+$ T cells were located throughout the tumor parenchyma (**Figure 2G**), and tumors were heavily infiltrated by macrophages that were faintly positive for tdT (**Figure 2H**). Moreover, a small number of macrophages had tdT^+ vesicles, suggesting phagocytosis of tumor cells. Together, these data demonstrate that Treg cells actively suppress immune destruction of established tumors.

Lung-tissue Treg cells are contained within tumor-associated tertiary lymphoid structures

We next investigated Treg cell localization in tumor-bearing lungs. Tumors in 20-wk KP-F mice had few infiltrating Treg cells and, instead, most Treg cells (>80-fold increase) were located in perivascular immune cell patches resembling TLS (**Figure 3A** and **B**). These structures also contained $CD11c^+$ dendritic cells (DCs) and $B220^+$ B cells, two cell types that have the potential to interact directly with Treg cells (**Figure 3C**). TA-TLS have been observed in patients with lung adenocarcinoma (Fridman et al., 2012), but not in animal tumor models. Therefore, we quantified the extent to which TLS were associated with tumors in this model and identified whether they displayed features of TA-TLS in human cancers.

Because tumors span several hundred microns, we reasoned that analyses of thin (5 μm) lung sections might underestimate the presence of TLS in tumor-bearing lungs. Therefore, we quantified the presence of TLS in 30 μm thick sections of tumor-bearing lungs from 8 mice and counted the number of tumors that were associated with TLS in three *in silico*-reconstructed tumor-bearing lung lobes (**Figure 3D**). Analysis of the 30 μm sections revealed ~60% (18/31) of tumors were directly associated with at least one TLS (defined as B cell clusters of >10 cells directly associated with T cells), and analysis of the *in silico* reconstructed lungs showed at least one TLS associated with ~93% (70/75) of tumors analyzed (data not shown).

We next used IF to characterize the cellular and structural components of TLS in thick sections of tumor-bearing lungs. TLS varied greatly in size and complexity, although this may be due to the fact that individual sections only capture part of a given TLS. TA-TLS in human cancers can have B and T cell zones organized by follicular dendritic cells (FDCs) and fibroblastic reticular cells (FRCs). Similarly, in this model, mature TLS had clearly defined $B220^+$ B cell and $CD3^+$ T cell areas, which were distinct from the $NKX2.1^+$ tumor areas (**Figure 3E-I**). Moreover, TLS all contained Treg cells, which were primarily located in the T cell areas (**Figure 3E-II**). About 30% of the time, B cell areas in the TLS contained detectable $CR1^+$ cells with long processes that were morphologically similar to FDCs (**Figure 3E-III**). These cells also expressed the B-cell chemoattractant CXCL13 and made direct contact with B cells (**Figure 3E-III** and **Movie S2A**). We also observed many T cells in the T cell areas were in direct contact with ERTR-7^+ $CCL21^+$ FRC-like cells (**Figure 3E-IV** and **Movie S2B**). The presence of FRC- and FDC-like cells in TA-TLS suggests they could help to organize and support infiltrating B and T cells.

Human TA-TLS contain high endothelial venules (HEVs), which in LNs constitutively recruit B and T cells from the circulation (de Chaisemartin et al., 2011; Neyt et al., 2012). We noted prominent, large $CD31^+$ $PNAd^+$ HEV-like structures, many of which had T cells in their lumen associated with the vessel wall (**Figure 3E-V** and **Movie S2C**). This indicates that HEV-like structures could be recruiting circulating T cells into TA-TLS in this model, as has been hypothesized in humans. Together, these data demonstrate that TLS associated with LucOS-expressing lung adenocarcinomas have hallmarks of LNs and phenotypically mirror TA-TLS seen in cancer patients.

Tertiary lymphoid structures facilitate T cell entry into and activation in the tumor microenvironment

It has been speculated that TA-TLS may be a site for local activation of tumor-specific T cells (Goc et al., 2013), but this possibility remains untested. Therefore, we focused on examining the function of TA-TLS *in vivo*. Because LucOS/Cre LV encodes the antigenic portions of ova, we used ova-specific T cell receptor (TCR) transgenic (Tg) OT-I $CD45.1^+$ CD8 T cells to analyze homing to and antigen presentation in TA-TLS (outlined in **Figure 4A**). As a negative control, LCMV-specific P14 Tg $CD45.1^+$ CD8 T cells were used because their TCR recognizes an antigen not present in LucOS. The OT-I and P14 T cells were activated *in vitro* to generate memory T cells, which are more sensitive for the presence of antigens (Kaech and Ahmed, 2001). Next, the OT-I and P14 T cells were labeled with the cell proliferation dyes cell trace violet (CT-V) and eFluor670 (CT-670), respectively, mixed at a 1:1 ratio, and adoptively transferred into 20-wk tumor-bearing $CD45.2^+$ KP-F mice or control non-tumor bearing $CD45.2^+$ P-F mice. On days 2 and 3 following transfer, homing, proliferation, and activation status were assessed by FACS and IF. When OT-I and P14 T cells were transferred to control mice, neither cell type appreciably entered the lung tissue, consistent with a lack of TLS in these mice (**Figure 4B**). In contrast, upon transfer into tumor-bearing hosts, both OT-I and P14 T cells entered the lung tissue. This suggests that like LNs, TLS in this model have the capacity to recruit activated T cells from the circulation. Both P14 and OT-I T cells were found in the lung tissue, but by IF a greater fraction of the OT-I T cells were located in the TLS (**Figure 4C** and **Figure S5A**).

Furthermore, OT-I T cells were observed interacting with DCs in the T cell areas of the TLS (**Figure 4D**). To determine whether these contacts were functionally relevant, we assessed whether OT-I and P14 T cells form immunologic synapses *in vivo* with DCs. Sections were stained with γ-tubulin (a marker of the microtubule organizing center, MTOC) and CD11c, and immunologic synapses were quantified based on MTOC position and interaction with a DC (**Figure S5B**). In cells forming synapses, the MTOC is repositioned to lie behind the synapse, and as such, can be used to determine the direction a T cell is oriented (Billadeau et al., 2007). Using this metric, along with the accumulation of cell proliferation dye (which non-specifically labels cellular protein) at the T cell-DC interface, OT-I T cells formed 2.7-fold more synapses relative to P14 T cells in TLS (**Figure 4E**). A similar increase was seen amongst OT-I T cells transferred into LucOS/Cre LV-infected vs. Cre LV-infected recipients, which have tumors that do not express LucOS (data not shown). Therefore, while OT-I and P14 T cells were both recruited into tumor-bearing lungs, OT-I T cells preferentially interacted with DCs in TLS. This interaction had a meaningful effect on the OT-I T cells as they upregulated CD69, an early marker of T cell activation, and proliferated within lung tissue, while P14 T cells did not (**Figure 4F**). Similar activation and proliferation patterns were seen in the tumor-draining mLN, but not in the in iLN, spleen, or the lung circulation (**Figure 4F** and data not shown). OT-I T cells did not upregulate CD69 or proliferate in the lung tissue or mLN when transferred into control P-F mice (data not shown). These data clearly demonstrate that infiltrating T cells can interact with tumor antigens in both the mLN and the TA-TLS.

Because some DCs in the TLS could have been directly infected by LucOS/Cre LV (20 wks prior) and, thus, their presentation of antigens might not be tumor specific, we analyzed DCs in KPT-F mice for the presence of tdT by IF. As the highly-active and ubiquitously-expressed CAG promoter drives tdT expression after Cre-mediated recombination in KPT-F mice (Madisen et al., 2010), direct infection of any cell type results in strong tdT signal. Twenty weeks after LucOS/Cre LV infection, directly infected round $CD11c^+$ macrophages were easily identified based on an abundant tdT signal, similar in intensity to tumor cells (data not shown). In contrast, some $CD11c^+$ DCs (distinguished from macrophages based on smaller size and dendritic morphology; Thornton et al., 2012) had faint signal for tdT in TA-TLS in KPT-F mice, implying these cells had phagocytosed tumor-derived products (**Figure 4G**). Additionally, we sorted lung tissue DCs from tumor-bearing lungs and confirmed they could present tumor-derived antigens to naïve OT-I CD8 T cells *in vitro* (**Figure S5C-D**). Together, these data demonstrate that much like the tumor-draining LN, tumor-associated TLS in this tumor model are functional structures capable of recruiting circulating CD8 T cells and facilitating their interactions with antigen-presenting DCs.

Local immune responses in tumor-associated tertiary lymphoid structures after Treg cell depletion

We next assessed the impact of Treg cell depletion on tumor-associated TLS. The area of the lung covered by TLS from ~20-wk LucOS/Cre LV-infected KP-F mice expanded ~7-fold in the 12 days after Treg cell depletion (**Figure 5A**). However, because it was unclear whether this increase was due to local lymphocyte expansion or recruitment, we analyzed TA-TLS for signs of immune activity at early time points following Treg cell depletion. Antigen-

driven lymphocyte activation is strongly correlated with cell division; therefore, we treated mice with the nucleoside analog bromodeoxyuridine (BrdU) 4 hours before sacrifice to label proliferation of lymphocytes. IHC analysis showed that the proportion of proliferating lymphocytes in TLS was increased at days 4 and 6 after Treg cell depletion (**Figure 5B and S6A**). Moreover, analysis of BrdU incorporation by FACS and IF revealed that the increased rates of proliferation were largely amongst $CD4^+$ and $CD8^+$ T cells in TLS, which increased ~5x- and ~10x-fold after Treg cell depletion (**Figures 5C-D**). Collectively, these data suggest that TA-TLS is a local site for T cell proliferation shortly after Treg cell depletion; although it is possible some T cells proliferated elsewhere and migrated to TA-TLS during the 4-hour window of our assay.

Treg cells directly regulate costimulatory molecules on DCs in SLOs (Kim et al., 2007), and, therefore, we reasoned that increased expression of costimulatory molecules on DCs immediately after Treg cell depletion could indicate sites of Treg cell function. CD80 (B7-1) and CD86 (B7-2) expression were examined on lung-tissue DCs 2 days after Treg cell depletion, when changes would most likely be due to direct effects in TLS. FACS analysis of day 2 and 6 Treg cell-depleted mice revealed that lung-tissue DCs had higher expression of CD80 and CD86 at day 2 after depletion (**Figure 5E**). These data are consistent with the possibility that, similar to their functions other SLOs, Treg cells in TA-TLS regulate DC function by reducing costimulatory levels. Furthermore, after Treg cell depletion, the overall microenvironment in the TA-TLS may become more immunostimulatory, promoting anti-tumor responses by T cells.

Local Treg cell depletion triggers anti-tumor responses targeting established lung adenocarcinomas

Intraperitoneal DT treatment of tumor-bearing KP-F mice causes acute systemic Treg cell depletion throughout the mouse. To verify that Treg cells in the local microenvironment of the lung suppress anti-tumor responses, we treated mice with repeated low doses of intratracheal DT, to deplete Treg cells locally within the lung. 20-wk LucOS/Cre LV-infected KP-F mice were treated with 6 daily doses of 50 ng DT IT. IT administration of DT did not result in LN enlargement, with the exception of the lung-draining mLN, and no morbidity was observed (data not shown). Local Treg cell depletion triggered immune infiltration of ~80% of lung tumors (**Figure 5F and S6B**). Therefore, local Treg cell depletion was sufficient to trigger strong anti-tumor effects, consistent with the idea that Treg cells in the TLS (and possibly in the mLN) regulate local anti-tumor responses. Moreover, these data demonstrate that efficient, local Treg cell depletion could be an effective means for triggering endogenous anti-tumor immune responses, without the systemic toxicity associated with whole body Treg cell depletion.

Programmed antigen expression is not required for anti-tumor responses following Treg cell depletion

We next examined whether Treg cell depletion enhanced responses by the CD8 T cells targeting the potent T cell antigens in LucOS. Surprisingly, however, we found that the number of endogenous SIINFEKL-specific CD8 T cells (identified with SIINFEKL-loaded H2-K^b MHC I tetramers) was not dramatically altered by Treg cell depletion (**Figures 6A**).

Additionally, the responses of naïve T cell OT-I CD8 T cells transferred into tumor-bearing recipients were not enhanced by the absence of Treg cells (data not shown). These data suggested that programmed antigen expression by tumors was not required to elicit anti-tumor responses following Treg cell depletion. Thus, we infected KP-F and KP x *FoxP3*$^{IRES\text{-}RFP}$ (KP-RFP) mice with Cre LV (previously referred to as Lenti-X in Dupage et al., 2011), and ~18 wks later, were treated with DT. After 12 days, lung tumors were analyzed for infiltration by immune cells and evidence of tumor destruction. Treg cell depletion resulted in dramatic infiltration of lung tissues by CD45^{+} cells, particularly in the perivascular and peribronchiolar regions (data not shown). Moreover, ~75% of tumors in Treg cell-depleted mice (n=174 tumors from 10 mice) were moderately (immune infiltration in 30-50% of the tumor area) or severely (greater than 50%) infiltrated and most showed evidence of immune-mediated tumor disruption (**Figure 6B-C**). In contrast, ~20% of the tumors from DT-treated KP-RFP (n=45 tumors from 6 mice) mice had moderate or severe immune infiltration (**Figure 6B-C**). Similarly, only 10% of non-DT treated week 20 KP-F mice (n=58 tumors from 5 mice) had severe or moderate infiltration. These data clearly demonstrate that the anti-tumor response seen following Treg cell depletion does not require the programmed expression of strong tumor antigens by tumors.

DISCUSSION

It is thought that the intratumoral Treg cells in cancer patients have important roles in immunosuppression, but it has not been possible to functionally explore these roles in humans. Here we demonstrated that Treg cells regulate anti-tumor immune responses in TA-TLS in a mouse model of lung adenocarcinoma. We observed that TLS recruit T cells from the circulation and facilitate their interaction with tumor-antigen presenting DCs. Treg cells in TLS actively suppress potent anti-tumor responses and, thus, the TLS is a primary site for T cell expansion upon Treg cell depletion. Subsequently, T cells and macrophages infiltrate tumors, resulting in significant tumor destruction. Collectively, these data point to immunosuppressive Treg cell function within TLS as one mechanism that prevents anti-tumor responses and allows continued tumor development.

TA-TLS have been observed in several human cancer types (Fridman et al., 2012; Goc et al., 2013) but it is not known how they form or function. In this model, TA-TLS formed during the course of tumor development, and were closely associated with ~90% of the LucOS-expressing tumors. Interestingly, antigen expression by tumors might impact TLS formation as TLS in lungs from Cre LV infected mice appear larger and are located centrally in the lungs, distal to tumors (N.S.J. and T.J. unpublished data).

In most studies, the presence of TA-TLS correlates with better survival for cancer patients, suggesting TA-TLS have anti-tumor functions. However, one study found that high numbers of Treg cells in TA-TLS, but not the tumor parenchyma, correlate with poor survival of breast cancer patients (Gobert et al., 2009). It has been difficult to study the function of TA-TLS, including how immunosuppressive pathways, like Treg cells, influence anti-tumor responses from within these structures. In this model, we observed that Treg cells are prominent in TA-TLS and that, upon Treg cell depletion, T cells within TA-TLS proliferate, coincident with tumor infiltration. Thus, we propose that TA-TLS may serve both pro- and

anti-tumor functions depending on the state of disease progression as well as the presence of immunosuppressive cell types, including Treg cells. However, TA-TLS also probably facilitate influx of new effector T cells into the tumor site following Treg cell depletion through HEVs, and amplify the anti-tumor response. Therefore, TA-TLS could be intimately involved in many aspects of the anti-tumor immune response, both at steady state and following therapeutic interventions.

The data presented here do not exclude the possibility that Treg cells in this model also suppress anti-tumor responses in the tumor-draining mLN. In contrast, because tumor-antigens are presented in TA-TLS and the mLN, regulation of anti-tumor immune responses likely requires immunosuppression at both sites. Because Treg cells function through a variety of mechanisms (Josefowicz et al., 2012), Treg cells in TA-TLS and the mLN could rely on distinct effector pathways. Consistent with this idea, Treg cells in TA-TLS were phenotypically more activated and expressed higher levels of multiple effector molecules. For example, Treg cells in our model (and others) express higher amounts of CTLA-4 in the tumor microenvironment compared to the tumor-draining LN (Marabelle et al., 2013; McDermott et al., 2014; Selby et al., 2013; Simpson et al., 2013). In the steady state, Treg cells use CTLA-4 to reduce the amounts of costimulatory proteins on DCs, thus inhibiting T cell activation and preventing autoimmunity (Qureshi et al., 2011; Wing et al., 2008). Likewise, Treg cells in TLS could use CTLA-4 to regulate anti-tumor responses through DCs. TA-TLS Treg cells also expressed high amounts of CD39, which, along with CD73, produces adenosine, a potent T cell inhibitor (Antonioli et al., 2013). Interestingly, chemical inhibition of CD39 has been shown to reduce early tumor growth in a Kras-driven *Atg5*-deficient mouse lung cancer model, possibly through Treg cell function (Rao et al., 2014). Further investigation will be required to more firmly establish the functional importance of these and other effector pathways active in Treg cells in TLS and to determine whether these pathways can be therapeutically exploited to improve anti-tumor immune responses.

CD8 T cell responses against the strong ova-antigen in LucOS were not dramatically enhanced by Treg cell depletion. This is perhaps because Treg cells preferentially suppress responses by T cells that have weak, lower-affinity interactions with their cognate antigen (Pace et al., 2012), more like those seen with self- or tumor-antigens (Aleksic et al., 2012). Therefore, in addition to Cre-derived antigens, after Treg cell depletion, T cells may also have been responding to self-antigens expressed by tumors in this model. Over- and abnormally expressed (non-mutated) antigens are frequent targets in human cancer (Finn, 2008), and advanced lung tumors in KP mice can express embryonic proteins and proteins normally found other locations, such as the gut (Snyder et al., 2013). Responses against these antigens would be suppressed under steady state conditions, but it is possible that Treg cell depletion permits responses by T cells with low affinity for these tumor-associated antigens. Identification of the types of tumor antigens recognized by T cells following Treg cell depletion will be helpful for guiding the development of future immune-based therapies.

Immune checkpoint blockers have enormous potential for treating a variety of types of human cancers, but positive clinical responses correlate with immune-related adverse events (Pardoll, 2012). As immune checkpoint pathways are important for preventing naturally-occurring autoimmune diseases, immunotherapies walk a fine line between promoting

strong anti-cancer effects and minimizing autoimmune toxicity. Treg cells are prime immunotherapeutic targets. In our model, systemic Treg cell depletion unleashed a powerful anti-tumor response, but also resulted in significant morbidity. Therefore, it seems possible that the autoimmune response triggered by systemic Treg cell depletion in patients could be difficult to control once initiated. This concern underscores the need to identify mechanisms for localized therapeutic depletion or targeted blockade of Treg cells in the tumor microenvironment. For example, some CTLA-4 antibodies can deplete intratumoral Treg cells, and treatment of metastatic melanoma patients with a Treg cell-depleting antibody ipilimumab provides an increase in overall survival, while treatment with a non-depleting antibody tremelimumab does not (Hodi et al., 2010; Ribas et al., 2013; Marabelle et al., 2013; McDermott et al., 2014; Selby et al., 2013; Simpson et al., 2013). From a therapeutic standpoint, specifically targeting immunosuppressive mediators in TA-TLS (like Treg cells) could make it possible to promote local anti-tumor responses and maintain immune homeostasis outside of the tumor microenvironment. Our study supports the development of additional targets for local Treg cell inhibition within the tumor microenvironment as a strategy that may provide safer, more effective therapy for patients with cancer.

EXPERIMENTAL PROCEDURES

Mice and treatments

KP and *Foxp3*$^{IRES\text{-}DTR\text{-}GFP}$ mice have been described (Dupage et al., 2011; Kim et al., 2007). OT-I TCR Tg and *Rosa26*$^{LSL\text{-}tdT}$ mice (B6.Cg-Gt(ROSA)26Sor$^{tm14(CAG\text{-}tdTomato)Hze/J}$) were purchased from Jackson Laboratory (Jax, Bar Harbor, ME) and P14 TCR Tg mice from Taconic (Hudson, NY). For systemic T_{reg} depletion, mice were injected IP with 50 ng / g DT in PBS on days 0 and 1 (2 doses). For lung-specific T_{reg} depletion, mice were treated with 50 ng DT IT in 50-100 μL PBS on days 0-5 (6 doses). IT DT was well tolerated by mice, and no morbidity or mortality was observed. Furthermore, IT DT did not trigger splenomegaly or lymphadenopathy, except in the lung-draining mediastinal LN (data not shown). Details of BrdU labeling, *in vivo* labeling and MRI imaging are in Supplemental Experimental Procedures. All studies were performed under an Institutional Animal Care and Use Committee- and Massachusetts Institute of Technology Committee on Animal Care-approved animal protocol. Mice were assessed for morbidity according to MIT division of comparative medicine (DCM) guidelines and were always humanely sacrificed prior to natural expiration.

Lentiviral production

Mice were infected IT with 2.5-5×10^4 PFU of Cre or LucOS/Cre LV to initiate tumors. Details of the viruses and production are in Supplemental Experimental Procedures.

Tissue isolation, Immunohistochemistry and Immunofluorescence

Lungs were isolated, flushed with bronchoalveolar lavage and/or lung circulatory perfusion, then allocated for IHC, IF, FACS and/or CLARITY. For IHC and IF, tissues were preserved overnight using PLP fixative, then embedded in paraffin (IHC) or cryoprotected with 30% sucrose/PBS (IF) and embedded in optimum cutting temperature (O.C.T.) compound (VWR,

Radnor, PA). Details of isolation, fixation, and IF/IHC staining are in Supplemental Experimental Procedures.

Confocal imaging

Images were acquired on an Olympus FV1200 Laser Scanning Confocal Microscope or a Nikon A1R Ultra-Fast Spectral Scanning Confocal Microscope with 10x, 20x, and 30x objectives and analyzed with ImageJ (NIH, Bethesda, MD) and Photoshop CS4 (Adobe Systems Inc, San Jose, CA). For whole lung reconstructions, individual sections were manually aligned using ImageJ and photoshop as detailed in Supplemental Experimental Procedures.

Flow cytometry

Spleens and LNs were processed as described (Joshi et al., 2007). Lungs were prepared using a gentleMACS dissociator and C tubes (Miltenyi biotech, San Diego, CA), as described in Supplemental Experimental Procedures. Samples were analyzed using an LSR II (BD) and FlowJo software (Treestar, Ashland, OR). Cell sorting was performed on a FACSAria III (BD).

Statistical analyses and quantifications

p-values from unpaired two-tailed student's T-tests were used for all statistical comparisons. Tumor destruction based on the disruption of tumor morphology and infiltration by $CD45^+$ immune cells was scored as described in Supplemental Experimental Procedures.

In vitro T cell activation and adoptive transfer

Splenocytes from OT-I or P14 TCR Tg mice were stimulated *in vitro*, stained with cell proliferation dyes and mixed at a 1:1 ratio, as detailed in the supplemental experimental materials. $1\text{-}5x10^6$ cells were then transferred IV into ~20-wk LucOS/Cre LV-infected recipient 45.2 KP-F mice.

Quantifying the percent BrdU+ from IHC sections

Sections of lungs were stained for BrdU by IHC, counterstained, and imaged using an Aperio Slide scanner (Leica). TA-TLS (distinct clusters of lymphocytes associated with blood vessels) were cropped using photoshop. Cropped images were quantified by Cell profiler for nuclei and BrdU+ cells to determine the fraction of proliferating lymphocytes.

Supplementary Material

Refer to Web version on PubMed Central for supplementary material.

ACKNOWLEDGMENTS

We thank Professor Alexander Rudensky (Memorial Sloan-Kettering Cancer Center) for the generous gift of $Foxp3^{DTR\text{-}GFP}$ mice and Jacks' lab members for reviewing the manuscript. We also thank Swanson Biotechnology Center (SBC): Kathleen Cormier in the Hope Babette Tang (1983) Histology Facility, Eliza Vasile and Jeff Wyckoff in the Microscopy Facility, Scott Malstrom in the Animal Imaging & Preclinical Testing Core Facility, Glenn Paradis in the Flow cytometry facility, and the KI Media Facility. This work was supported by an NCI Cancer Center Support Grant P30-CA14051 and grants from the Howard Hughes Medical Institute (T.J.), 1

U54 CA126515-01 (T.J.), R01 – CA185020-01 (T.J.), and T32 GM007753 (A.L.) from the NIH, the Damon Runyon Cancer Foundation (N.S.J.), the Margaret A. Cunningham Immune Mechanisms in Cancer Research Fellowship Award (N.S.J.) and the Lung Cancer Research Foundation (N.S.J.). T.J. is a Howard Hughes Investigator and a Daniel K. Ludwig Scholar. This paper is dedicated to Professor Herman Eisen and Officer Sean Collier, for his caring service to the MIT community and for his sacrifice.

REFERENCES

Aleksic M, Liddy N, Molloy PE, Pumphrey N, Vuidepot A, Chang KM, Jakobsen BK. Different affinity windows for virus and cancer-specific T-cell receptors: implications for therapeutic strategies. European journal of immunology. 2012; 42:3174–3179. [PubMed: 22949370]

Antonioli L, Pacher P, Vizi ES, Hasko G. CD39 and CD73 in immunity and inflammation. Trends in molecular medicine. 2013; 19:355–367. [PubMed: 23601906]

Beyersdorf N, Ding X, Tietze JK, Hanke T. Characterization of mouse CD4 T cell subsets defined by expression of KLRG1. European journal of immunology. 2007; 37:3445–3454. [PubMed: 18034419]

Billadeau DD, Nolz JC, Gomez TS. Regulation of T-cell activation by the cytoskeleton. Nature reviews. 2007; 7:131–143.

Boissonnas A, Scholer-Dahirel A, Simon-Blancal V, Pace L, Valet F, Kissenpfennig A, Sparwasser T, Malissen B, Fetler L, Amigorena S. Foxp3+ T cells induce perforin-dependent dendritic cell death in tumor-draining lymph nodes. Immunity. 2010; 32:266–278. [PubMed: 20137985]

Bos PD, Plitas G, Rudra D, Lee SY, Rudensky AY. Transient regulatory T cell ablation deters oncogene-driven breast cancer and enhances radiotherapy. J Exp Med. 2013; 210:2435–2466. [PubMed: 24127486]

Campbell DJ, Koch MA. Phenotypical and functional specialization of FOXP3+ regulatory T cells. Nature reviews. 2011; 11:119–130.

Cheng G, Yuan X, Tsai MS, Podack ER, Yu A, Malek TR. IL-2 receptor signaling is essential for the development of Klrg1+ terminally differentiated T regulatory cells. J Immunol. 2012; 189:1780–1791. [PubMed: 22786769]

Chung K, Wallace J, Kim SY, Kalyanasundaram S, Andalman AS, Davidson TJ, Mirzabekov JJ, Zalocusky KA, Mattis J, Denisin AK, et al. Structural and molecular interrogation of intact biological systems. Nature. 2013; 497:332–337. [PubMed: 23575631]

de Chaisemartin L, Goc J, Damotte D, Validire P, Magdeleinat P, Alifano M, Cremer I, Fridman WH, Sautes-Fridman C, Dieu-Nosjean MC. Characterization of chemokines and adhesion molecules associated with T cell presence in tertiary lymphoid structures in human lung cancer. Cancer research. 2011; 71:6391–6399. [PubMed: 21900403]

Dieu-Nosjean MC, Antoine M, Danel C, Heudes D, Wislez M, Poulot V, Rabbe N, Laurans L, Tartour E, de Chaisemartin L, et al. Long-term survival for patients with non-small-cell lung cancer with intratumoral lymphoid structures. Journal of clinical oncology : official journal of the American Society of Clinical Oncology. 2008; 26:4410–4417. [PubMed: 18802153]

Dupage M, Cheung AF, Mazumdar C, Winslow MM, Bronson RT, Schmidt LM, Crowley D, Chen J, Jacks T. Endogenous T cell responses to antigens expressed in lung adenocarcinomas delay malignant tumor progression. Cancer cell. 2011; 19:72–85. [PubMed: 21251614]

DuPage M, Jacks T. Genetically engineered mouse models of cancer reveal new insights about the antitumor immune response. Curr Opin Immunol. 2013; 25:192–199. [PubMed: 23465466]

DuPage M, Mazumdar C, Schmidt LM, Cheung AF, Jacks T. Expression of tumour-specific antigens underlies cancer immunoediting. Nature. 2012; 482:405–409. [PubMed: 22318517]

Feuerer M, Hill JA, Kretschmer K, von Boehmer H, Mathis D, Benoist C. Genomic definition of multiple ex vivo regulatory T cell subphenotypes. Proceedings of the National Academy of Sciences of the United States of America. 2010; 107:5919–5924. [PubMed: 20231436]

Finn OJ. Cancer immunology. The New England journal of medicine. 2008; 358:2704–2715. [PubMed: 18565863]

Fridman WH, Pages F, Sautes-Fridman C, Galon J. The immune contexture in human tumours: impact on clinical outcome. Nature reviews. 2012; 12:298–306.

Gobert M, Treilleux I, Bendriss-Vermare N, Bachelot T, Goddard-Leon S, Arfi V, Biota C, Doffin AC, Durand I, Olive D, et al. Regulatory T cells recruited through CCL22/CCR4 are selectively activated in lymphoid infiltrates surrounding primary breast tumors and lead to an adverse clinical outcome. Cancer research. 2009; 69:2000–2009. [PubMed: 19244125]

Goc J, Fridman WH, Sautes-Fridman C, Dieu-Nosjean MC. Characteristics of tertiary lymphoid structures in primary cancers. Oncoimmunology. 2013; 2:e26836. [PubMed: 24498556]

Hayes SA, Hudson AL, Clarke SJ, Molloy MP, Howell VM. From mice to men: GEMMs as trial patients for new NSCLC therapies. Seminars in cell & developmental biology. 2014; 27:118–127. [PubMed: 24718320]

Hodi FS, O'Day SJ, McDermott DF, Weber RW, Sosman JA, Haanen JB, Gonzalez R, Robert C, Schadendorf D, Hassel JC, et al. Improved survival with ipilimumab in patients with metastatic melanoma. The New England journal of medicine. 2010; 363:711–723. [PubMed: 20525992]

Jemal A, Siegel R, Xu J, Ward E. Cancer statistics, 2010. CA Cancer J Clin. 2010; 60:277–300. [PubMed: 20610543]

Josefowicz SZ, Lu LF, Rudensky AY. Regulatory T cells: mechanisms of differentiation and function. Annual review of immunology. 2012; 30:531–564.

Joshi NS, Cui W, Chandele A, Lee HK, Urso DR, Hagman J, Gapin L, Kaech SM. Inflammation directs memory precursor and short-lived effector CD8(+) T cell fates via the graded expression of T-bet transcription factor. Immunity. 2007; 27:281–295. [PubMed: 17723218]

Kaech SM, Ahmed R. Memory CD8+ T cell differentiation: initial antigen encounter triggers a developmental program in naive cells. Nature immunology. 2001; 2:415–422. [PubMed: 11323695]

Kim JM, Rasmussen JP, Rudensky AY. Regulatory T cells prevent catastrophic autoimmunity throughout the lifespan of mice. Nature immunology. 2007; 8:191–197. [PubMed: 17136045]

Kwon MC, Berns A. Mouse models for lung cancer. Mol Oncol. 2013; 7:165–177. [PubMed: 23481268]

Lin W, Truong N, Grossman WJ, Haribhai D, Williams CB, Wang J, Martin MG, Chatila TA. Allergic dysregulation and hyperimmunoglobulinemia E in Foxp3 mutant mice. The Journal of allergy and clinical immunology. 2005; 116:1106–1115. [PubMed: 16275384]

Madisen L, Zwingman TA, Sunkin SM, Oh SW, Zariwala HA, Gu H, Ng LL, Palmiter RD, Hawrylycz MJ, Jones AR, et al. A robust and high-throughput Cre reporting and characterization system for the whole mouse brain. Nature neuroscience. 2010; 13:133–140. [PubMed: 20023653]

Marabelle A, Kohrt H, Sagiv-Barfi I, Ajami B, Axtell RC, Zhou G, Rajapaksa R, Green MR, Torchia J, Brody J, et al. Depleting tumor-specific Tregs at a single site eradicates disseminated tumors. J Clin Invest. 2013; 123:2447–2463. [PubMed: 23728179]

McDermott D, Lebbe C, Hodi FS, Maio M, Weber JS, Wolchok JD, Thompson JA, Balch CM. Durable benefit and the potential for long-term survival with immunotherapy in advanced melanoma. Cancer treatment reviews. 2014

Neyt K, Perros F, GeurtsvanKessel CH, Hammad H, Lambrecht BN. Tertiary lymphoid organs in infection and autoimmunity. Trends in immunology. 2012; 33:297–305. [PubMed: 22622061]

Pace L, Tempez A, Arnold-Schrauf C, Lemaitre F, Bousso P, Fetler L, Sparwasser T, Amigorena S. Regulatory T cells increase the avidity of primary CD8+ T cell responses and promote memory. Science. 2012; 338:532–536. [PubMed: 23112334]

Pardoll DM. The blockade of immune checkpoints in cancer immunotherapy. Nature reviews. 2012; 12:252–264.

Qureshi OS, Zheng Y, Nakamura K, Attridge K, Manzotti C, Schmidt EM, Baker J, Jeffery LE, Kaur S, Briggs Z, et al. Trans endocytosis of CD80 and CD86: a molecular basis for the cell-extrinsic function of CTLA-4. Science. 2011; 332:600–603. [PubMed: 21474713]

Raez LE, Fein S, Podack ER. Lung cancer immunotherapy. Clinical medicine & research. 2005; 3:221–228. [PubMed: 16303887]

Rajasagi M, Shukla SA, Fritsch EF, Keskin DB, DeLuca D, Carmona E, Zhang W, Sougnez C, Cibulskis K, Sidney J, et al. Systematic identification of personal tumor-specific neoantigens in chronic lymphocytic leukemia. Blood. 2014; 124:453–462. [PubMed: 24891321]

Rao S, Tortola L, Perlot T, Wirnsberger G, Novatchkova M, Nitsch R, Sykacek P, Frank L, Schramek D, Komnenovic V, et al. A dual role for autophagy in a murine model of lung cancer. Nature communications. 2014; 5:3056.

Ribas A, Kefford R, Marshall MA, Punt CJ, Haanen JB, Marmol M, Garbe C, Gogas H, Schachter J, Linette G, et al. Phase III randomized clinical trial comparing tremelimumab with standard-of-care chemotherapy in patients with advanced melanoma. Journal of clinical oncology : official journal of the American Society of Clinical Oncology. 2013; 31:616–622. [PubMed: 23295794]

Robbins SH, Tessmer MS, van Kaer L, Brossay L. Direct effects of T-bet and MHC class I expression, but not STAT1, on peripheral NK cell maturation. European journal of immunology. 2005; 35:757–765. [PubMed: 15719366]

Sakaguchi S. Naturally arising CD4+ regulatory t cells for immunologic self-tolerance and negative control of immune responses. Annual review of immunology. 2004; 22:531–562.

Sather BD, Treuting P, Perdue N, Miazgowicz M, Fontenot JD, Rudensky AY, Campbell DJ. Altering the distribution of Foxp3(+) regulatory T cells results in tissue-specific inflammatory disease. J Exp Med. 2007; 204:1335–1347. [PubMed: 17548521]

Selby MJ, Engelhardt JJ, Quigley M, Henning KA, Chen T, Srinivasan M, Korman AJ. Anti-CTLA-4 antibodies of IgG2a isotype enhance antitumor activity through reduction of intratumoral regulatory T cells. Cancer immunology research. 2013; 1:32–42. [PubMed: 24777248]

Simpson TR, Li F, Montalvo-Ortiz W, Sepulveda MA, Bergerhoff K, Arce F, Roddie C, Henry JY, Yagita H, Wolchok JD, et al. Fc-dependent depletion of tumor-infiltrating regulatory T cells co-defines the efficacy of anti-CTLA-4 therapy against melanoma. J Exp Med. 2013; 210:1695–1710. [PubMed: 23897981]

Snyder EL, Watanabe H, Magendantz M, Hoersch S, Chen TA, Wang DG, Crowley D, Whittaker CA, Meyerson M, Kimura S, et al. Nkx2-1 represses a latent gastric differentiation program in lung adenocarcinoma. Molecular cell. 2013; 50:185–199. [PubMed: 23523371]

Suffia I, Reckling SK, Salay G, Belkaid Y. A role for CD103 in the retention of CD4+CD25+ Treg and control of Leishmania major infection. J Immunol. 2005; 174:5444–5455. [PubMed: 15845457]

Teng MW, Ngiow SF, von Scheidt B, McLaughlin N, Sparwasser T, Smyth MJ. Conditional regulatory T-cell depletion releases adaptive immunity preventing carcinogenesis and suppressing established tumor growth. Cancer research. 2010; 70:7800–7809. [PubMed: 20924111]

Thornton EE, Looney MR, Bose O, Sen D, Sheppard D, Locksley R, Huang X, Krummel MF. Spatiotemporally separated antigen uptake by alveolar dendritic cells and airway presentation to T cells in the lung. J Exp Med. 2012; 209:1183–1199. [PubMed: 22585735]

Vogelstein B, Papadopoulos N, Velculescu VE, Zhou S, Diaz LA Jr. Kinzler KW. Cancer genome landscapes. Science. 2013; 339:1546–1558. [PubMed: 23539594]

Wing K, Onishi Y, Prieto-Martin P, Yamaguchi T, Miyara M, Fehervari Z, Nomura T, Sakaguchi S. CTLA-4 control over Foxp3+ regulatory T cell function. Science. 2008; 322:271–275. [PubMed: 18845758]

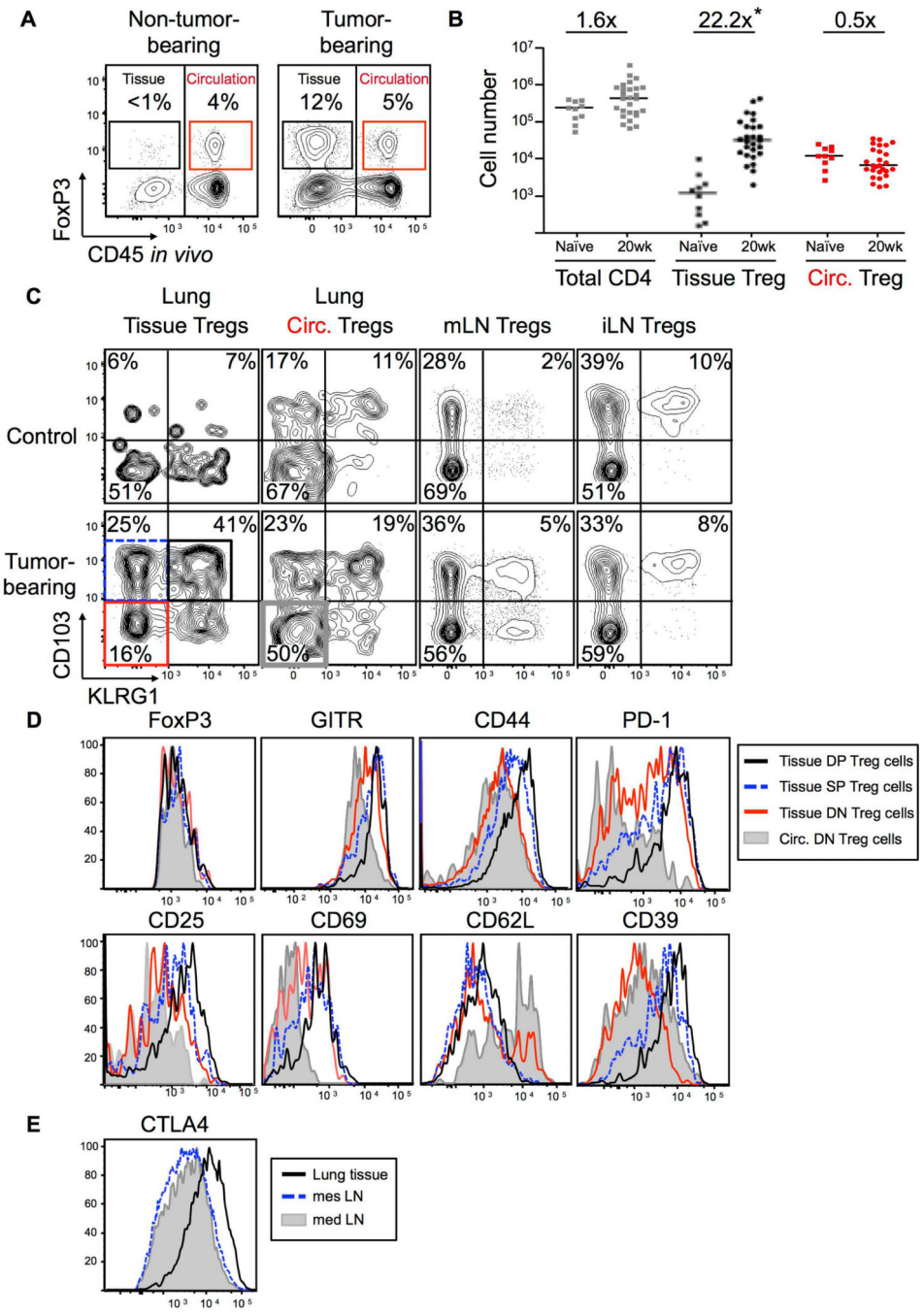

Figure 1. Treg cells in tumor-bearing lungs have an activated phenotype

KP-F and P-F (control) mice were analyzed ~20 wks (18-24 wks) after LucOS/Cre LV infection by flow cytometry.

(A) FACS plots gated on lung $CD4^+$ T cells. Tissue (black) and circulating (red) $FoxP3^+$ Treg cell frequency indicated. Note, control and uninfected (naïve) lungs were indistinguishable. n > 30 mice.

(B) Graph of total CD4 T cell and tissue and circulating Treg cell numbers in lungs from naïve (n=11) and tumor-bearing (20 wk, n=30) animals. Median and fold difference indicated. *, p = 0.03.

(C) CD103 and KLRG1 on the Treg cell populations in **1A**. n > 30 mice.

(D) Expression of indicated markers by circulating DN (filled gray line) and tissue DN, SP, and DP Treg cells (red, dashed blue, and black lines, respectively). Gated as in **1C**. n = 9-35 mice.

(E) CTLA-4 expression by mLN (gray filled line), mesenteric (mes) LN (dashed blue line) and lung tissue Treg cells (black line). n = 7 mice.

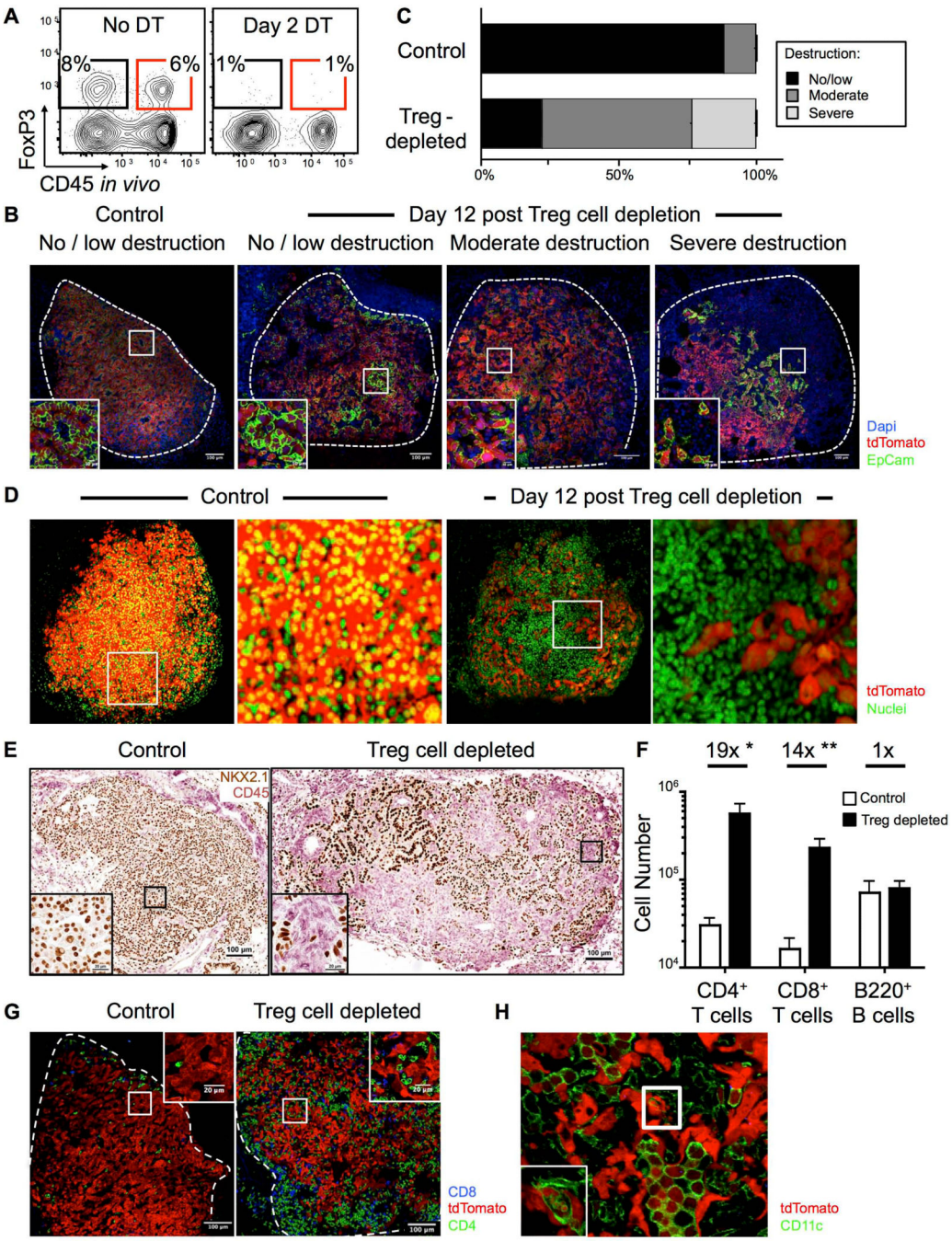

Figure 2. Treg cells maintain immune quiescence in advanced tumors

~18-20-wk LucOS/Cre LV-infected KP-F (A) or KPT-F (B-H) mice were treated 1x (A) or 2x (B-H) with DT (IP; 50ng/g) and analyzed 2 (A) or 12 (B-H) days later.

(A) FACS plots show lung $CD4^+$ T cells, gated as in **1A**. n > 6 mice.

(B) Confocal IF images show range (no/low, moderate, or severe) of tumor destruction in untreated (left panel) and Treg cell-depleted (right 3 panels) mice. Red: $tdTomato^+$; green: EpCAM; blue: Dapi; Dashed line: tumor border.

(C) Quantitation of tumor destruction from images in **2C**. n = 85/13 control and 108/17 Treg cell-depleted tumors/mice.
(D) Control (left panels) and Treg cell-depleted (right panels) lungs were optically cleared using CLARITY. Images show optical slices through tumors. Red: tdTomato$^+$; green: YO-PRO-1. See also **Movie S1**. n = 15/7 control and 10/3 Treg cell-depleted tumors/mice.
(E) IHC images show control and Treg cell-depleted tumors for lung (NKX2.1, brown) and immune (CD45, pink) cells. n = 71/11 control and 55/9 Treg cell-depleted tumors/mice.
(F) Graph of median lung-tissue CD4$^+$ and CD8$^+$ (Thy1.2$^+$) T cell and (B220$^+$ CD19$^+$) B cell numbers in Treg cell-depleted (black bars, n=6) and control mice (white bars, n=5) ± SEM. *, p=0.0150. **, p=0.0175.
(G) Confocal IF images show control (n=39) and Treg cell-depleted (n=15) tumors. Red: tdTomato$^+$; green: CD4; blue: CD8 T cells.
(H) Confocal IF image shows Treg cell-depleted tumor. Red: tdTomato$^+$; green: CD11c$^+$ macrophage (large round cells). Inset optical slice of macrophage with tdT$^+$ vesicles (z-depth different than larger image). n = 4 mice.

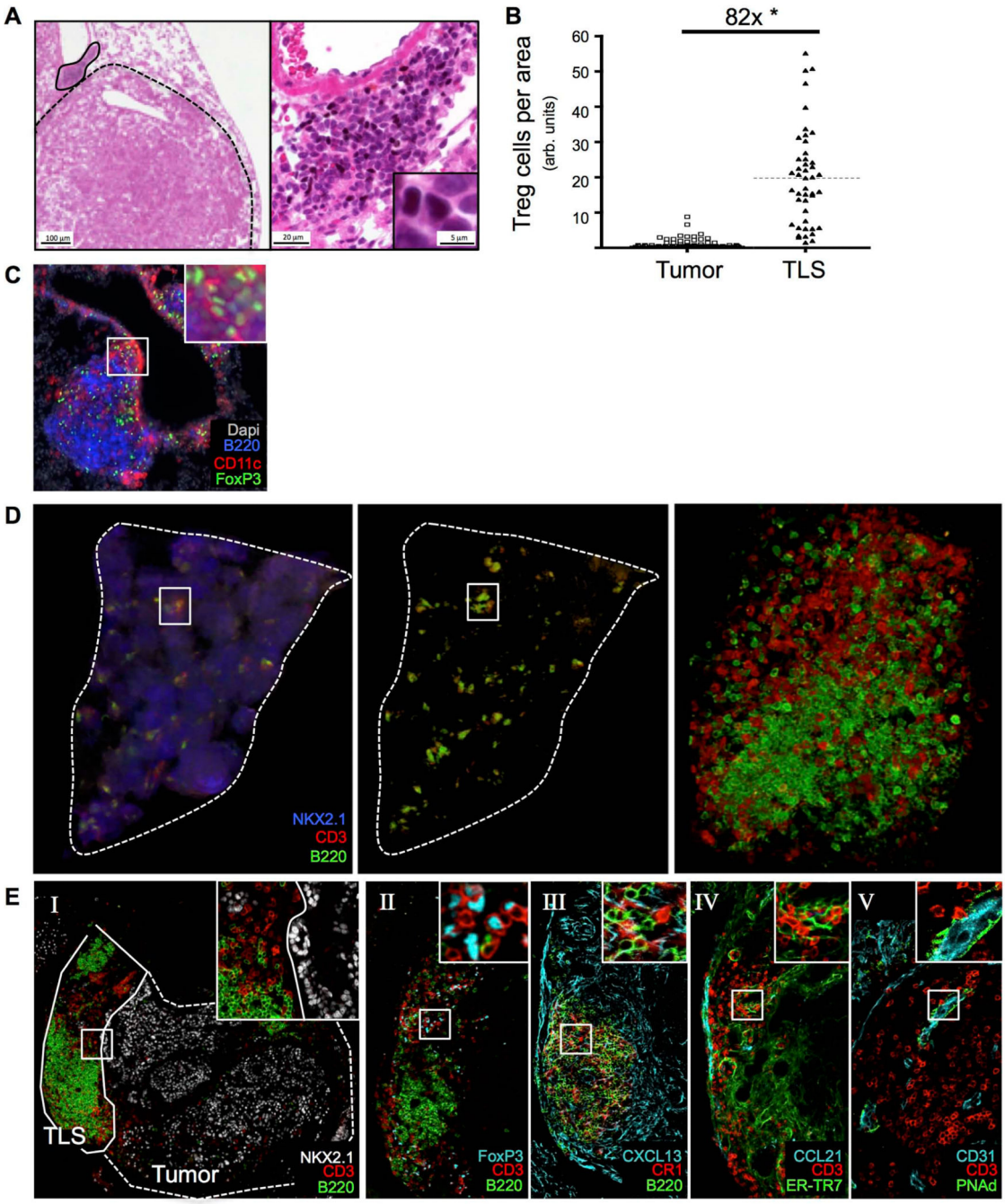

Figure 3. Treg cells in tumor-bearing lungs are located in tumor-associated TLS

KP-F or KPT-F mice were analyzed 18-20 wks after LucOS/Cre LV infection.

(A) IHC images show FoxP3 (black), hematoxylin (blue) and eosin (pink). Tumor, dashed line; TLS, solid line. Left panel, 4x. Right panel, 20x. n = 10 mice.

(B) Median Treg cell number in tumor (n=88) and TLS (n=45) from 9 mice. Normalized by pixel area. *, $p=3.89\times10^{-25}$.

(C) IF image shows TLS. Red, CD11c; Green, FoxP3; Blue, B220; White, Dapi. n = 6 mice.

(D) 3-D rendering of in silico reconstructed tumor-bearing lung lobe. ~20 IF sections (50μM, ~1 mm depth) imaged by confocal microscopy. Blue, NKX2.1; red, CD3; green, B220. Center panel same as left with NXK2.1 removed. Right panel, TLS in box. n = 3 mice.

(E) Confocal IF images show TLS in serial stained sections (30 μm) stained for indicated markers. I, tumor, dashed line; TLS, solid line. n = 16 mice.

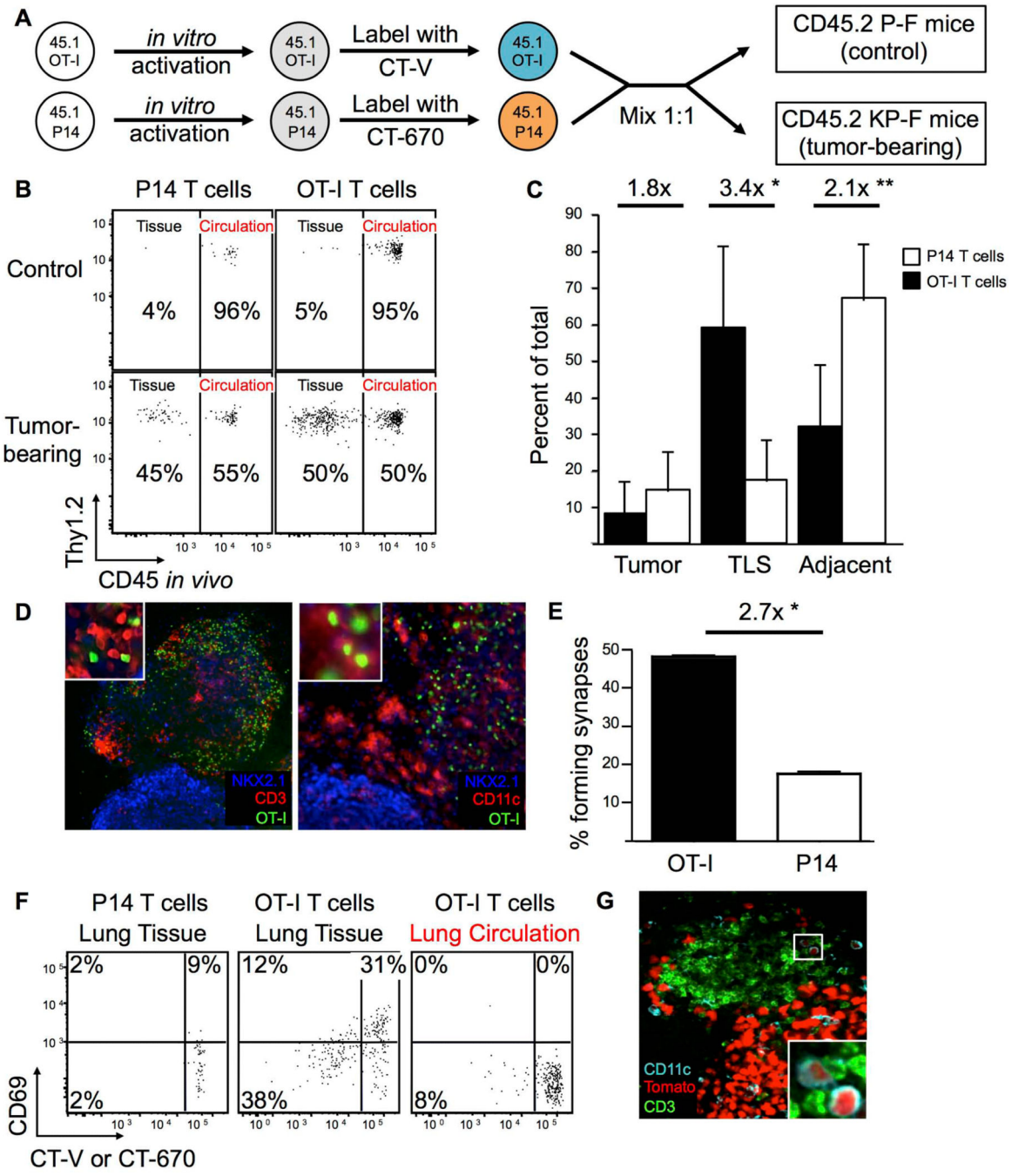

Figure 4. TLS serves as a local site of tumor antigen presentation

(A) Schematic diagram for **B-F**. *In vitro*-activated CT-670$^+$ P14 and CT-V$^+$ OT I Tg CD45.1$^+$ CD8$^+$ T cells were transferred into ~20-wk LucOS/Cre LV-infected CD45.2$^+$ tumor-bearing KP-F and control P-F recipients.

(B) FACS plots show lung CD45.1$^+$ CD8$^+$ P14 and OT-I T cells 2-3 days after transfer. n >12 per group.

(C) Graph showing the median fraction (± SEM) of transferred OT-I (black bars, n = 620) or P14 (white bars, n = 238) CD8 T cells in the indicated tissue (see also **Figure S5A**). *, $p = 1.89\times10^{-3}$. **, $p = 3.59\times10^{-3}$.

(D) Confocal IF images of TLS. Green: CT-V (OT-I T cells); blue: NKX2.1, and red: CD3 (left panel, n = 13) or CD11c (right panel, n >20).

(E) Graph showing the mean fraction (± SEM) of OT-I (black bar, n = 231) or P14 (white bar, n = 122) T cells forming synapses (see also **Figure S5B**). *, $p=5.62\times10^{-11}$.

(F) FACS plots showing transferred P14 or OT-I $CD8^+$ T cells (gated as in **5B**). n >12 recipients.

(G) Confocal IF image shows tumor/TLS in ~20 wk LucOS/Cre LV-infected KPT-F mouse. Green, CD3; cyan, CD11c (DCs are small cells); red, tdTomato. Note, signal intensity difference between tumor cells and DCs. n = 5 mice.

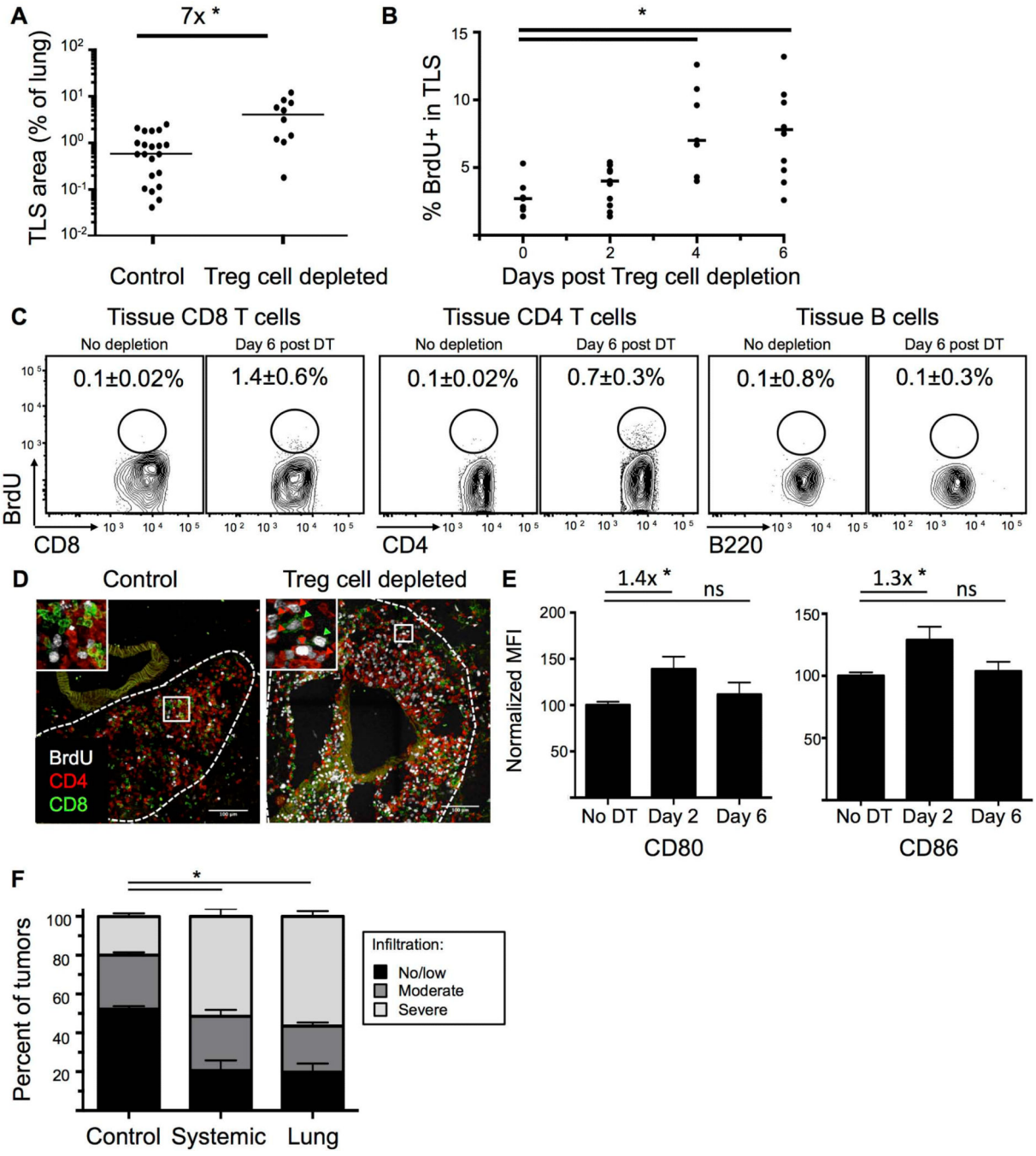

Figure 5. TLS is a site of immune activation following Treg cell depletion

~20-wk LucOS/Cre LV-infected KP-F mice were treated IP (A-F) or IT (F) with DT. (B-D) mice treated with BrdU to label proliferating cells.

(A) Graph quantifying TLS / lung size of 22 control and 10 day-12 Treg cell-depleted mice. *, $p=1.8\times10^{-4}$.

(B) Graph shows the percent of $BrdU^{+}$ lymphocytes in TLS after Treg cell depletion. Day 0, no DT. Points are the average of lymphocytes in all the TLS in a section. Bar: median. See also **Figure S6A**. n=7, days 0 and 4 and n=11, days 2 and 6. *, $p<0.005$.

(C) FACS plots show BrdU staining in lung-tissue CD8 and CD4 ($FoxP3^{neg}$) T cells and $B220^+$ $CD19^+$ B cells. Average of 3 control and 6 T_{reg}-depleted mice ± SEM.
(D) Confocal IF images show control (n=18/9 TLS/mice) and day 6 Treg cell-depleted (n=57/12) TLS. Green, CD8; red, CD4; white, BrdU. Arrowheads: $BrdU^+$ CD8 (green) and CD4 (red) T cells.
(E) Graphs show median (± SEM) CD80 and CD86 MFI (median fluorescence intensity) on lung-tissue $CD11b^+$ $CD11c^+$ $MHCII^+$ DCs. n=8, no DT; n=12, day 2; n=13, day 6 post DT. Fold change indicated. ns=non-significant. *, $p<0.05$.
(F) Graph shows blind quantification of IHC on lung sections from control (n=630/23), day-12 IP DT treated (systemic depletion, n=136/15 tumors/mice), and day-12 IT DT treated (lung-restricted depletion, n=266/11) mice stained for CD45 and NKX2.1. no/little, < 30%; moderate 30-50%; severe, >50% $CD45^+$ cell infiltration. *, $p<0.005$.

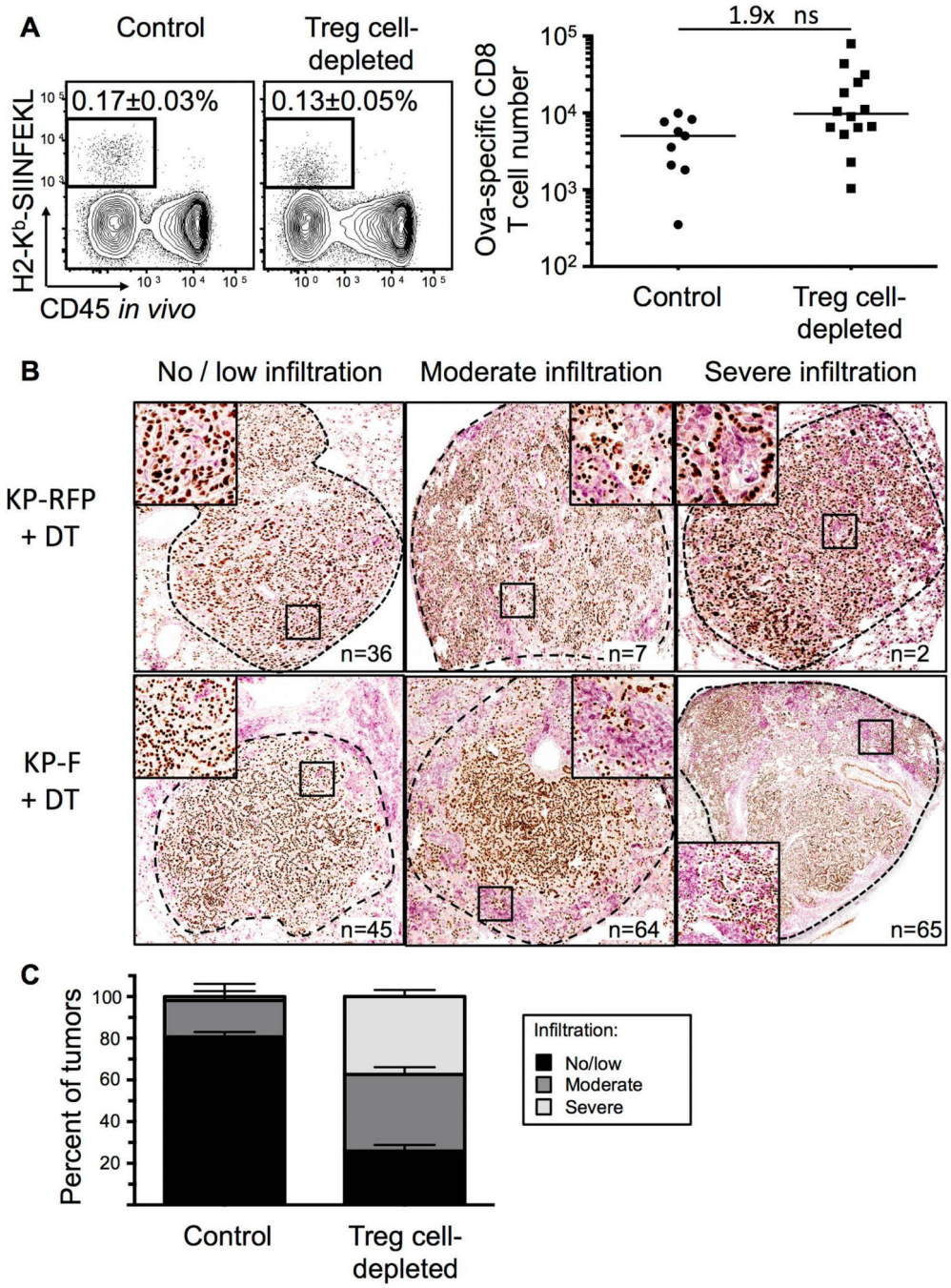

Figure 6. Overt antigen expression by tumors not required for anti-tumor response after Treg cell depletion

(A) FACS plots show and graph show endogenous ova-specific $CD8^+$ T cells (identified with H2-K^b-SIINFEKL tetramer) in control (n=9) and day 12 T_{reg}- depleted (IP; n=14) ~20-wk LucOS/Cre LV-infected KP-F mice. Plots gated on $CD8^+$ T cells. Median frequency of total ± SEM indicated on plots. ns=non-significant. Note, no tetramer staining was observed in Cre LV-infected mice.

(B) IHC images show NKX2.1 (brown) and CD45 (pink) in ~18-wk Cre LV-infected KP-F (n=15) and KP-RFP (control, n=6) mice 12 days after IP DT. no/little, < 30%; moderate 30-50%; severe, >50% $CD45^+$ cell infiltration. n = tumor number.
(C) Graph quantifying IHC in **6B.** Control includes tumors from DT-treated KP RFP (n= 45 tumors/6 mice) and untreated KP-F (n=58 tumors/5 mice). n = 174 Treg cell-depleted tumors from 10 mice.